

Ultra-low damping of the translational motion of a composite graphite particle in a magneto-gravitational trap

Connor E. Murphy,¹ Cody Jessup,¹ Tahereh Naderishahab,¹ Leonardo R. Werneck,² Zachariah B. Etienne,^{2,3,4} and Brian D'Urso^{*1}

¹*Department of Physics, Montana State University, Bozeman, MT*

²*Department of Physics, University of Idaho, Moscow, ID*

³*Department of Physics and Astronomy, West Virginia University, Morgantown, WV*

⁴*Center for Gravitational Waves and Cosmology, Chestnut Ridge Research Building, Morgantown, WV*

(*Electronic mail: durso@montana.edu)

(Dated: 24 June 2025)

We demonstrate an ultra-low dissipation, one-dimensional mechanical oscillator formed by levitating a millimeter-scale composite graphite particle in a room-temperature magneto-gravitational trap. The trap's magnetic field geometry, based on a linear quadrupole, eliminates first-order field gradients in the axial direction, yielding a low oscillation frequency with negligibly low eddy-current losses. Direct ring-down measurements under vacuum compare the damping of the vertical and axial motion; while the vertical motion damps in seconds, the axial motion shows no apparent damping in 24 hours. Analysis reveals that this dramatic difference in damping is a result of the symmetry of the magnetic field and the anisotropy of the trap strength. The results are remarkably robust, demonstrating a potential platform for inertial and gravitational sensing.

Levitated optomechanical systems consisting of an optically-trapped silica nanosphere have been used to demonstrate cooling to the quantum ground state of a kilohertz harmonic oscillator by taking advantage of the low damping in these systems.¹⁻⁴ For inertial and gravitational sensing, systems with larger masses and lower oscillation frequencies can be beneficial.⁵⁻⁸ To minimize noise, the low damping and isolation from the surrounding environment of levitated systems are still critical.⁹ In particular, magneto-gravitational traps (MGTs) have been used to levitate diamagnetic particles ranging in size from about 1 μm ^{10,11} to 300 μm .¹²

MGTs offer an especially attractive solution for creating low-frequency, large mass harmonic oscillators for inertial and gravitational sensing due to their static trapping mechanism and capability of trapping large masses. A MGT geometry similar to the one discussed here has previously been used to levitate charged 50 μm borosilicate spheres with the aid of a vertical electric field.⁵ However, that system has high damping rates due to the movement of mirror charges in the conductive pole pieces.¹³

Graphite is a promising material for magnetic levitation due to its strong diamagnetic susceptibility. However, graphite is also conductive, giving rise to eddy-current damping when it moves through a magnetic field gradient.¹⁴ Various methods have been used to try to characterize and combat this issue, such as mixing graphite powder with a non-conducting epoxy,¹⁵ cutting the graphite with a conductive geometry,¹⁶ coating graphite beads with silica and embedding them in wax,¹⁷ and studying rotation of a graphite rotor in an axially-symmetric magnetic field.¹⁸ While each of these methods decreases damping, none is able to make it negligibly small. The approach taken here combines the method of using a composite graphite particle with a MGT geometry that effectively creates a one-dimensional harmonic oscillator with so little dissipation that ambient noise causes the amplitude of its motion to increase more than damping causes it to decrease.

The magneto-gravitational trap used in this experiment is made by sandwiching two nickel-plated NdFeB magnets between four Hiperco 50A (iron-cobalt alloy) pole pieces, as shown in Fig. 1, to create a magnetic field which is dominated by a linear quadrupole component. This results in a strong trapping force in the transverse (x) and vertical (y) directions, and a weak trapping force in the axial (z) direction. Furthermore, there is reason to expect that the damping in the z direction could be weak because the symmetry of the trap results in no linear magnetic field gradients in the z direction at the center of the trap.

Using notation from a multipole expansion of the trap magnetic field¹⁰ inside a MGT that takes advantage of the symmetries of the system, we write the magnetic field as

$$\vec{B} = - \begin{bmatrix} \frac{1}{4} \frac{a_2}{y_0} \sqrt{\frac{15}{\pi}} y + \frac{1}{12} \frac{a_3}{y_0^2} \sqrt{\frac{21}{2\pi}} (4z^2 - y^2 - 3x^2) \\ \frac{1}{4} \frac{a_2}{y_0} \sqrt{\frac{15}{\pi}} x - \frac{1}{6} \frac{a_3}{y_0^2} \sqrt{\frac{21}{2\pi}} xy \\ \frac{2}{3} \frac{a_3}{y_0} \sqrt{\frac{21}{2\pi}} xz \end{bmatrix}, \quad (1)$$

where a_2 and a_3 parameterize the strength of the quadrupole and hexapole terms, respectively, and $y_0 = 6.14 \times 10^{-4}$ m is a dimensional scaling factor representative of the trap dimensions. Higher-order terms have been dropped because they are not important for the motion studied here.

A diamagnetic particle in a magnetic field and subject to the Earth's gravitational acceleration g has potential energy

$$U = - \frac{\chi m}{2\mu_0 \rho} B^2 - mgy, \quad (2)$$

where μ_0 is the permeability of free space, χ is the volume magnetic susceptibility of the particle, ρ is its mass density, and m is its mass. When trapped, the contribution from gravity gives rise to an offset in the vertical equilibrium position, y_{eq} , which in our system is empirically determined to

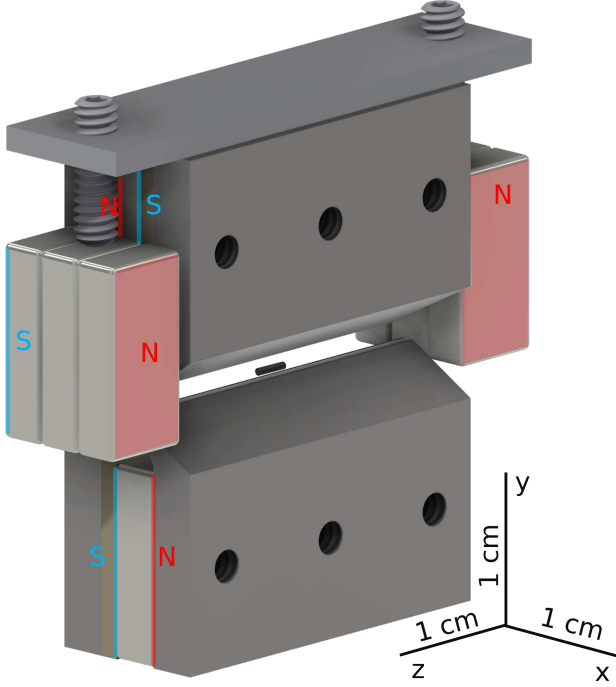


FIG. 1. A schematic of the magneto-gravitational trap used for levitating a graphite particle. Set screws are used to adjust the height of the 3-magnet stacks on both axial ends of the trap in order to create a low-frequency axial trapping potential. North (N) and south (S) pole labels are shown to describe the magnet orientations relative to each other. The dark cylinder in the gap between the pole pieces represents the trapped composite graphite rod.

be $y_{eq} = -0.10$ mm. Trapping in the z direction is a result of the combination of this gravitational offset and (for $x = 0$) the x component of the magnetic field, which is plotted in Fig. 2.

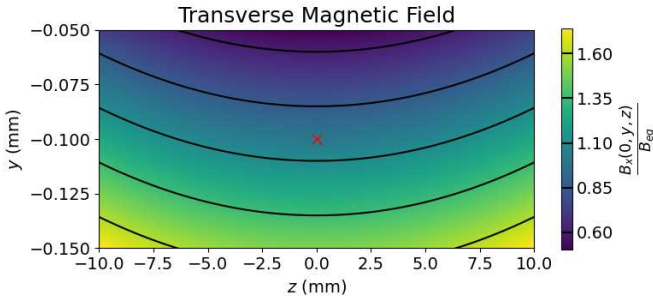


FIG. 2. A plot of the relative transverse magnetic field, $B_x(x=0)$, near the particle's equilibrium position (shown by the red "x"). Note the difference in scale between z and y , indicative of the high level of anisotropy in the trap. The y -axis is shown magnified 100 times relative to the z -axis.

The frequency of harmonic oscillation along each trap axis $\zeta = x, y, \text{ or } z$ is given by¹⁰

$$\omega_\zeta^2 = \frac{-\chi}{2\rho\mu_0} \frac{\partial^2 B^2}{\partial \zeta^2}, \quad (3)$$

which for $x = 0$ and $y \rightarrow y_{eq} + y$ gives

$$\omega_y \approx \frac{-\chi}{2\rho\mu_0} \left(\frac{15}{8\pi} \frac{a_2^2}{y_0^2} - \frac{315}{8\pi} \frac{a_2 a_3}{y_0^3} y_{eq} \right), \quad (4)$$

$$\omega_z \approx \frac{-\chi}{2\rho\mu_0} \left(\frac{210}{\pi} \frac{a_2 a_3}{y_0^3} y_{eq} \right), \quad (5)$$

where we have neglected terms of order ζ^2 and higher. Since $\omega_z \ll \omega_y$, we drop the second term in Eq. (4) in further analysis.

By combining Eqs. (1), (4), and (5) and dropping all but the lowest-order terms in each partial derivative, we note that $\frac{\partial B_x}{\partial y}$ is a constant and can write $\frac{\partial B_x}{\partial z}$ as:

$$\frac{\partial B_x}{\partial z} = \left(\frac{\omega_z}{\omega_y} \right)^2 \left(\frac{z}{y_{eq}} \right) \frac{\partial B_x}{\partial y}. \quad (6)$$

Other components of the field do not contribute a restoring force since $B_y = B_z = 0$ for $x = 0$. Critically, for low damping in the z direction, the appearance of the ratio of the frequencies squared is a result of the lack of a linear field gradient in the z direction at the equilibrium position.

To estimate the effect of eddy currents within the particle due to its motion in the B_x field gradients, we model the particle as a loop of wire in the y - z plane with resistance R and transverse cross-sectional area A_x .

Assuming that the oscillations are weakly damped ($\Gamma_\zeta \ll \omega_\zeta$), the eddy-current damping rate for the system can then be estimated from the ratio of the Ohmic power loss due to induced current I to the energy of the oscillator E averaged over one period as

$$\Gamma_\zeta = \frac{\langle I^2 R \rangle_\zeta}{\langle E \rangle_\zeta} = \frac{A_x^2}{R} \frac{\left\langle \frac{\partial B_x}{\partial \zeta}^2 \zeta^2 \right\rangle_\zeta}{m\omega_\zeta^2 \zeta_{rms}^2}. \quad (7)$$

Eq. (7), as discussed in more detail in supplementary material Sec. A, gives the vertical damping rate in the system as

$$\Gamma_y = \left(\frac{\partial B_x}{\partial y} \right)^2 \frac{A_x^2}{mR}, \quad (8)$$

and we can determine the axial damping rate by combining Eq. (6) with Eq. (7) to get:

$$\Gamma_z = \left(\frac{\partial B_x}{\partial y} \right)^2 \left(\frac{\omega_z}{\omega_y} \right)^2 \frac{A_x^2 \zeta_{rms}^2}{2mRy_{eq}^2}. \quad (9)$$

Finally, the relationship between Γ_z and Γ_y is

$$\Gamma_z = \left(\frac{\omega_z}{\omega_y} \right)^4 \frac{\zeta_{rms}^2}{2y_{eq}^2} \Gamma_y, \quad (10)$$

The appearance of the ratio of the oscillation frequencies to the fourth power suggests the possibility of dramatically lower damping in the weakly-confined axial direction when compared to the much more strongly-confined vertical direction.

The levitated test mass is a 2.4-mm-long segment of 0.5 mm-diameter Pentel HB pencil lead, shown in Fig. 3. The composition of the pencil lead is approximately 68 % graphite, 26 % clay, and 5 % wax,¹⁹ which likely increases its resistivity compared to pure graphite.²⁰ Prior to levitation, the ends of the particle are lapped smooth.

Multiple precautions are taken to minimize electrostatic sources of damping. First, the tips of the trap’s pole pieces are covered with 25 μm -thick copper foil to decrease surface patch potentials. Second, an Am-241 ionizing radiation source is directed at the trapping region for several minutes at atmospheric pressure to neutralize any net charge accumulated on the particle and adjacent surfaces. The axial trapping potential is then adjusted by moving two magnet stacks at the axial ends of the trap (see Fig. 1), which allows for fine-tuning of the axial frequency and ensures a stable potential well.

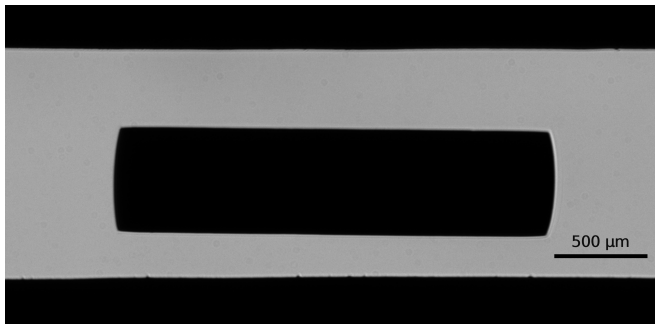


FIG. 3. An image of a piece of ~ 0.5 mm-diameter piece of Pentel HB pencil lead levitated in a MGT imaged along the x -axis. The top and bottom black sections are the top and bottom pole pieces. The pixel size is calibrated to be 3.45 μm .

The position of the particle in the y - z plane is recorded by capturing images of the particle back-illuminated with light from a pulsed blue LED and imaged onto a CMOS camera (Basler acA2440-75um) with a Mitutoyo 1X telecentric objective lens. Cross-correlation based image analysis²¹ is used to precisely determine the apparent particle displacement. For axial (vertical) motion analysis, the recorded frame rate is 150 Hz (550 Hz) with an illumination time of 25 μs in each frame.

To decrease damping of the particle’s motion due to residual gas, the vacuum chamber enclosing the trap is baked at $\sim 100^\circ\text{C}$ under high vacuum, followed by pumping with ion and titanium sublimation pumps. The pressure in the chamber varied from approximately 3×10^{-8} Torr to 6×10^{-8} Torr over the course of the experiments, as recorded on the ion pump controller.

The vacuum chamber and optics are built on a platform that is suspended on four air isolation mounts for vibration isolation. The axial tilt of the platform is actively stabilized to an rms variation of 0.054 μrad to prevent the particle from drifting.²²

We analyze two recordings of the particle’s motion. In the first data set, 24 hours of motion are recorded after the particle is excited axially to an amplitude of approximately 1.1 mm by manually tilting the table on resonance with its axial motion.

In the second, the vertical motion of the particle is excited by striking the vacuum chamber with a rubber mallet, resulting in an amplitude of approximately 24 μm , but the data is only recorded for 30 s due to the rapid damping of the vertical motion. The short damping time of the vertical motion does not permit time for the axial tilt to restabilize; recording after axial excitation did not begin until after the axial tilt had restabilized.

The damping rate for each axis of motion was calculated by finding the kinetic energy of the motion in each direction as a function of time after excitation. This was done by fitting the data points surrounding each zero-crossing in displacement to a cubic function, then analytically differentiating to obtain a velocity (see supplementary material Sec. B). Fig. 4 illustrates the motion of the particle as well as exponential fits to the kinetic energy in each degree of freedom over time. Note the

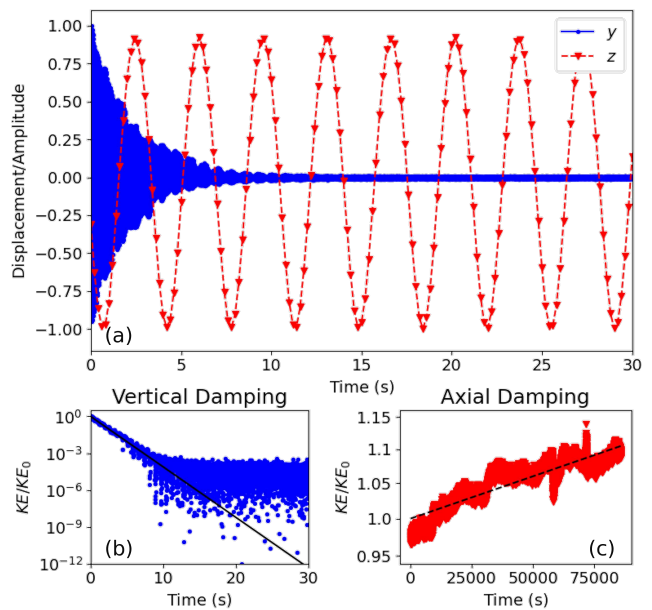


FIG. 4. Plot (a) displays several oscillation cycles in the vertical (y) motion and a few cycles in the axial (z) motion of the levitated graphite. Plot (b) shows the kinetic-energy fit to the particle’s y -motion over 30 seconds, and plot (c) shows the kinetic-energy fit to the particle’s z -motion over 24 hours, both with a logarithmic vertical scale. The exponential fits to the energy are displayed as black lines. The vertical damping rate was measured to be $\Gamma_y = 0.946(3) \text{ s}^{-1}$ and the effective axial damping rate, which varied greatly from run to run, was found in this particular measurement to be about $\Gamma_z \approx -1.2 \times 10^{-6} \text{ s}^{-1}$. The negative value reflects the slow increase in energy, presumably due to environmental noise sources driving the nearly undamped motion.

drastic difference in damping rates between vertical and axial motions. The axial damping is so low that the system actually gains energy from its environment (e.g. through vibrations, as the initial amplitude is far above thermal equilibrium) over the course of 24 hours, demonstrating a negligible axial damping rate.

We can use the system parameters and Eq. (10) to estimate the axial damping rate due to eddy currents from the measured

vertical damping rate. We measured $z_{rms} = 7.9 \times 10^{-4}$ m from the axial damping data and $y_{eq} = -1.0 \times 10^{-4}$ m from Fig. 3. By interpolating around the peak values in the Fourier domain (see supplementary material Sec. C), the vertical and axial frequencies of motion were determined to be $\omega_y/(2\pi) = 40.3$ Hz and $\omega_z/(2\pi) = 0.281$ Hz. Combining these values together gives $\Gamma_z \approx 6.9 \times 10^{-8} \text{ s}^{-1}$, corresponding to a $1/e$ time of about 170 days. In practice, another damping mechanism such as eddy currents in the conductive pole pieces,²³ collisions between the particle and residual gas molecules,²⁴ or mirror charge movement in the pole pieces due to remaining charge on the particle¹³ may be the dominant (although still unseen) source of damping.

Eq. (10) shows how the field geometry of the MGT makes it possible to obtain ultra-low damping in one trap axis coincident with strong damping in the other two orthogonal axes (the transverse motion is not analyzed but is similar to the vertical motion). Having such strong dissipation in the vertical and transverse directions and such low dissipation in the axial direction damps any off-axis motion of the particle rapidly, effectively creating a one-dimensional oscillator without the need for active feedback cooling.¹⁷

It is interesting to note that these results were obtained without careful fine-tuning of the alignment of the pole pieces – similar results were obtained with two different instances of assembly of the trap by two different people as well as multiple graphite composite particles. Additionally, Fig. 3 shows that the particle had a noticeable tilt relative to the camera, which was leveled to the axial motion of the particle to within 0.1° . This indicates a low-damping result that is remarkably robust to misalignment.

Further improvements on the design might be made by adjusting the locations of the end-magnet stacks to further flatten the potential, or by implementing some other form of potential tuning.²⁵ Additionally, using a seismometer to measure vibrations and tilts in the table or the ground it rests on might help further characterize the forces driving the motion of the particle and lead to a more quantitative understanding of the damping rate in the system.

SUPPLEMENTARY MATERIAL

See the supplementary material that provides additional details on calculations and the techniques used to extract peak velocities and oscillation frequencies from the position data.

ACKNOWLEDGMENTS

This work was primarily supported by the National Science Foundation under Grant Nos. 1912083 and 2011783 (B.D.) and Grant Nos. 2011817 and 2227079 (Z.B.E.).

DATA AVAILABILITY STATEMENT

The data that support the findings of this study are available from the corresponding author upon reasonable request.

- ¹U. Delić, M. Reisenbauer, K. Dare, D. Grass, V. Vuletić, N. Kiesel, and M. Aspelmeyer, “Cooling of a levitated nanoparticle to the motional quantum ground state,” *Science* **367**, 892–895 (2020).
- ²F. Tebbenjohanns, M. L. Mattana, M. Rossi, M. Frimmer, and L. Novotny, “Quantum control of a nanoparticle optically levitated in cryogenic free space,” *Nature* **595**, 378–382 (2021).
- ³L. Magrini, P. Rosenzweig, C. Bach, A. Deutschmann-Olek, S. G. Hofer, S. Hong, N. Kiesel, A. Kugi, and M. Aspelmeyer, “Real-time optimal quantum control of mechanical motion at room temperature,” *Nature* **595**, 373–377 (2021).
- ⁴Y. Xu, Y.-H. Liu, C. Liu, and J.-Q. Liao, “Simultaneous ground-state cooling of two levitated nanoparticles by coherent scattering,” *Physical Review A* **109**, 053521 (2024).
- ⁵C. W. Lewandowski, T. D. Knowles, Z. B. Etienne, and B. D’Urso, “High-sensitivity accelerometry with a feedback-cooled magnetically levitated microsphere,” *Physical Review Applied* **15**, 014050 (2021).
- ⁶F. Monteiro, W. Li, G. Afek, C.-I. Li, M. Mossman, and D. C. Moore, “Force and acceleration sensing with optically levitated nanogram masses at microkelvin temperatures,” *Physical Review A* **101**, 053835 (2020).
- ⁷Y. Li, C. Li, J. Zhang, Y. Dong, and H. Hu, “Collective-motion-enhanced acceleration sensing via an optically levitated microsphere array,” *Physical Review Applied* **20**, 024018 (2023).
- ⁸Q. Wang, X. Ren, S. Jiao, X. Lei, S. Zhang, H. Liu, P. Luo, and L. Tu, “A diamagnetic levitation based inertial sensor for geophysical application,” *Sensors and Actuators A: Physical* **312**, 112122 (2020).
- ⁹C. Timberlake, G. Gasbarri, A. Vinante, A. Setter, and H. Ulbricht, “Acceleration sensing with magnetically levitated oscillators above a superconductor,” *Applied Physics Letters* **115** (2019).
- ¹⁰J.-F. Hsu, P. Ji, C. W. Lewandowski, and B. D’Urso, “Cooling the motion of diamond nanocrystals in a magneto-gravitational trap in high vacuum,” *Scientific reports* **6**, 30125 (2016).
- ¹¹B. R. Slezak, C. W. Lewandowski, J.-F. Hsu, and B. D’Urso, “Cooling the motion of a silica microsphere in a magneto-gravitational trap in ultra-high vacuum,” *New Journal of Physics* **20**, 063028 (2018).
- ¹²J. P. Houlton, M. L. Chen, M. D. Brubaker, K. A. Bertness, and C. T. Rogers, “Axisymmetric scalable magneto-gravitational trap for diamagnetic particle levitation,” *Review of Scientific Instruments* **89**, 125107 (2018), <https://doi.org/10.1063/1.5051667>.
- ¹³L. S. Brown and G. Gabrielse, “Geonium theory: Physics of a single electron or ion in a penning trap,” *Rev. Mod. Phys.* **58**, 233–311 (1986).
- ¹⁴X. Chen, A. Keşkekler, F. Alijani, and P. G. Steeneken, “Rigid body dynamics of diamagnetically levitating graphite resonators,” *Applied Physics Letters* **116** (2020).
- ¹⁵X. Chen, S. K. Ammu, K. Masania, P. G. Steeneken, and F. Alijani, “Diamagnetic composites for high-q levitating resonators,” *Advanced Science* **9**, 2203619 (2022).
- ¹⁶H. Xie, Y. Li, R. Li, Y. Leng, Y. Chen, L. Wang, D. Long, X. Bian, C.-K. Duan, P. Yin, *et al.*, “Suppressing mechanical dissipation of diamagnetically levitated oscillator via engineering conductive geometry,” *Physical Review Research* **5**, 013030 (2023).
- ¹⁷S. Tian, K. Jadeja, D. Kim, A. Hodges, G. Hermosa, C. Cusicanqui, R. Lecamwasam, J. Downes, and J. Twamley, “Feedback cooling of an insulating high-q diamagnetically levitated plate,” *Applied Physics Letters* **124** (2024).
- ¹⁸D. Kim, S. Tian, B. Calderoni, C. S. Jachimska, J. Downes, and J. Twamley, “A magnetically levitated conducting rotor with ultra-low rotational damping circumventing eddy loss,” *arXiv preprint arXiv:2505.09895* (2025).
- ¹⁹M. C. Sousa and J. W. Buchanan, “Observational models of graphite pencil materials,” in *Computer graphics forum*, Vol. 19 (Wiley Online Library, 2000) pp. 27–49.
- ²⁰A. Jain, “On the specific resistivity of graphite pieces of different types,” *Basic and Applied Engineering Research* **10**, 96–97 (2023).
- ²¹L. R. Werneck, C. Jessup, A. Brandenberger, T. Knowles, C. W. Lewandowski, M. Nolan, K. Sible, Z. B. Etienne, and B. D’Urso, “Cross-

- correlation image analysis for real-time single particle tracking," *Review of Scientific Instruments* **95**, 073708 (2024).
- ²²C. W. Lewandowski, T. D. Knowles, Z. B. Etienne, and B. D'Urso, "Active optical table tilt stabilization," *Review of Scientific Instruments* **91** (2020).
- ²³A. B. Matsko, S. P. Vyatchanin, and L. Yi, "On mechanical motion damping of a magnetically trapped diamagnetic particle," *Physics Letters A* **384**, 126643 (2020).
- ²⁴A. Cavalleri, G. Ciani, R. Dolesi, M. Hueller, D. Nicolodi, D. Tombolato, S. Vitale, P. J. Wass, and W. J. Weber, "Gas damping force noise on a macroscopic test body in an infinite gas reservoir," *Physics Letters A* **374**, 3365–3369 (2010).
- ²⁵D. Long, K. Tian, H. Xie, Y. Chen, Y. Sheng, P. Yin, and P. Huang, "Diamagnetically levitated force sensor with adjustable natural frequency between 0.5 and 21 Hz," *Journal of Applied Physics* **137** (2025).
- ²⁶F. Xiong, L. Guo, Z. Chen, A. Du, C. Li, and T. Wu, "Achievement of a vacuum-levitated metal mechanical oscillator with ultra-low damping rate at room temperature," *Communications Physics* **8**, 80 (2025).
- ²⁷A. Khodaei, K. Dare, A. Johnson, U. Delić, and M. Aspelmeyer, "Dry launching of silica nanoparticles in vacuum," *AIP Advances* **12** (2022).
- ²⁸A. Ashkin, J. M. Dziedzic, and T. Yamane, "Optical trapping and manipulation of single cells using infrared laser beams," *Nature* **330**, 769–771 (1987).
- ²⁹D. S. Bykov, P. Mestres, L. Dania, L. Schmöger, and T. E. Northup, "Direct loading of nanoparticles under high vacuum into a Paul trap for levitodynamical experiments," *Applied Physics Letters* **115** (2019).
- ³⁰X. Zhu, T. Wu, J. Yang, Z. Chen, L. Guo, H. Hu, Z. Fu, and C. Li, "Suppressing damping in a diamagnetically levitated dielectric sphere via charge neutralization," in *2023 IEEE SENSORS* (2023) pp. 1–4.

Ultra-low damping of the translational motion of a composite graphite particle in a magneto-gravitational trap:

Supplementary Information

Connor E. Murphy,¹ Cody Jessup,¹ Tahereh Naderishahab,¹ Leonardo R. Werneck,² Zachariah B. Etienne,^{2,3,4} and Brian D'Urso^{*1}

¹*Department of Physics, Montana State University, Bozeman, MT*

²*Department of Physics, University of Idaho, Moscow, ID*

³*Department of Physics and Astronomy, West Virginia University, Morgantown, WV*

⁴*Center for Gravitational Waves and Cosmology, Chestnut Ridge Research Building, Morgantown, WV*

(*Electronic mail: duroso@montana.edu)

SUPPLEMENTARY MATERIAL

A. Eddy Current Damping

To get from Eq. (7) to Eqs. (8) and (9) in the main text, we can express the long-term behavior of the system as

$$\ddot{y} = -\omega_y^2 y - \Gamma_y \dot{y} \quad (\text{S1})$$

$$\ddot{z} = -\omega_z^2 z - \Gamma_z(z) \dot{z}, \quad (\text{S2})$$

noting that in general Γ_z cannot be assumed to be independent of amplitude.

This relationship allows us to estimate the average energy and $I^2 R$ -losses for $\Gamma_\zeta \ll \omega_\zeta$. The average energy is given by

$$\begin{aligned} \langle E \rangle_\zeta &= \left\langle \frac{1}{2} m \omega_\zeta^2 \zeta^2 + \frac{1}{2} m \dot{\zeta}^2 \right\rangle_\zeta \\ &\approx \frac{1}{2} m \omega_\zeta^2 \langle \zeta_0^2 \cos^2 \omega_\zeta t + \zeta_0^2 \sin^2 \omega_\zeta t \rangle_\zeta \\ &= m \omega_\zeta^2 \zeta_{rms}^2, \end{aligned} \quad (\text{S3})$$

where ζ_0 is the amplitude of the motion at $t \approx 0$.

The current induced by the motion of the particle through a field gradient can be calculated using Faraday's law:

$$I = \frac{V}{R} = -\frac{A_x}{R} \frac{dB_x}{dt} = -\frac{A_x}{R} \frac{\partial B_x}{\partial \zeta} \dot{\zeta}. \quad (\text{S4})$$

The value $\langle \frac{\partial B_x}{\partial y} z^2 \rangle_y$ can trivially be calculated due to the fact that $\frac{\partial B_x}{\partial y}$ is approximately constant. For z , however, it is a little more complicated:

$$\begin{aligned} \left\langle \frac{\partial B_x}{\partial z} z^2 \right\rangle_z &= \left(\frac{\omega_z}{\omega_y} \right)^4 \frac{1}{y_{eq}^2} \langle z^2 z^2 \rangle_z \\ &\approx \left(\frac{\omega_z}{\omega_y} \right)^4 \frac{1}{y_{eq}^2} \langle z_0^4 \omega_z^2 \sin^2 \omega_z t \cos^2 \omega_z t \rangle_z \\ &= \left(\frac{\omega_z}{\omega_y} \right)^4 \frac{\omega_z^2 z_0^4}{8 y_{eq}^2}, \end{aligned} \quad (\text{S5})$$

which yields the form of Eq. (9) from the main text with the use of the substitution $z_{rms}^2 \approx \frac{1}{2} z_0^2$.

B. Kinetic Energy Analysis

To analyze the damping behavior of an oscillator, it is useful to be able to estimate its energy as a function of time. Since the system under study in this experiment is somewhat anharmonic, making a precise calculation of potential energy difficult, it is beneficial to analyze the kinetic energy of the particle over time.

Since the mass of the particle can be considered to be invariant in time, measuring velocity squared is sufficient to characterize the energy damping of the particle's motion.

The peak velocity every half-cycle was determined from the time-domain z -motion of the particle by fitting a cubic to a set of points around each zero-crossing, as shown in Fig. S1. The cubic fit can then be analytically differentiated to obtain a parabolic fit to the velocities, so that the vertex of each parabola estimates the peak velocity of the particle.

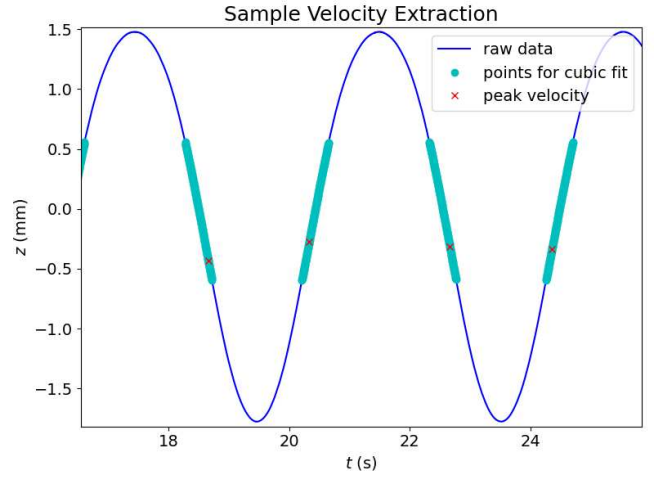


FIG. S1. An 8-second portion of axial displacement data shown to demonstrate the method used to calculate the kinetic energy for estimating damping rates. The fits shown use 200 points around each zero-crossing to fit a cubic to the data, allowing analytical differentiation to be used to calculate peak velocities.

The square of these peak velocities can then be plotted in time to estimate the damping rate for the z -motion of the particle, as shown in Fig. 4 in the main text.

The same method was used to find the peak velocities for the vertical motion, except that only 6 points were used in each fit due to the higher oscillation frequency.

C. Frequency Extraction

The natural frequencies of the oscillator along its three principle axes can be measured from the amplitude spectral density (ASD) of the particle's motion. This is done by interpolating a parabola to the three points around the peak in the ASD corresponding to the particle's natural frequency, as shown for z in Figure S2 and y in Figure S3.

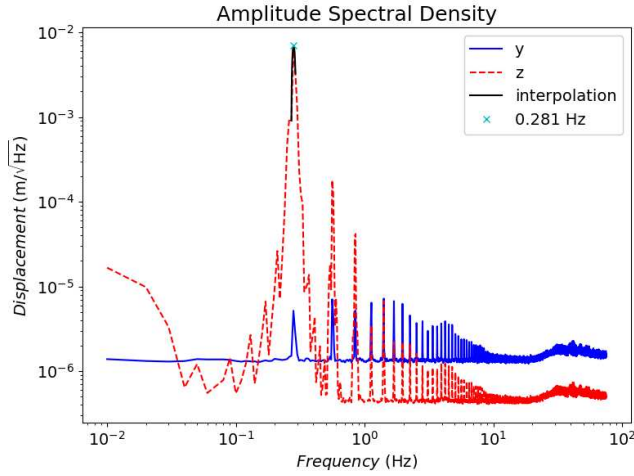


FIG. S2. Amplitude spectral density calculated by taking the Fourier transform of the 24-hour dataset used to analyze the z -ringdown of the particle's motion. The measured frequency is $\omega_z/(2\pi) = 0.281$ Hz.

The vertical motion can be seen to some extent in Figure S2, however, a better SNR can be obtained by looking at the y -ringdown obtained from the shorter data set with excited vertical motion shown in Figure S3.

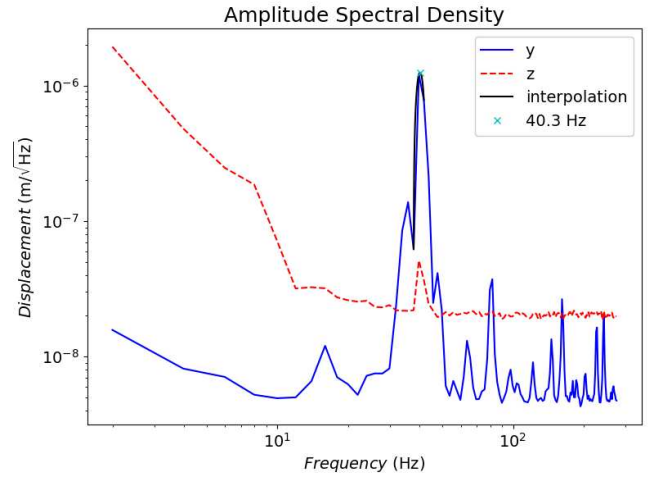


FIG. S3. Amplitude spectral density calculated by taking the Fourier transform of the 30-second dataset used to analyze the y -ringdown of the particle's motion. The measured frequency is $\omega_y/(2\pi) = 40.3$ Hz.